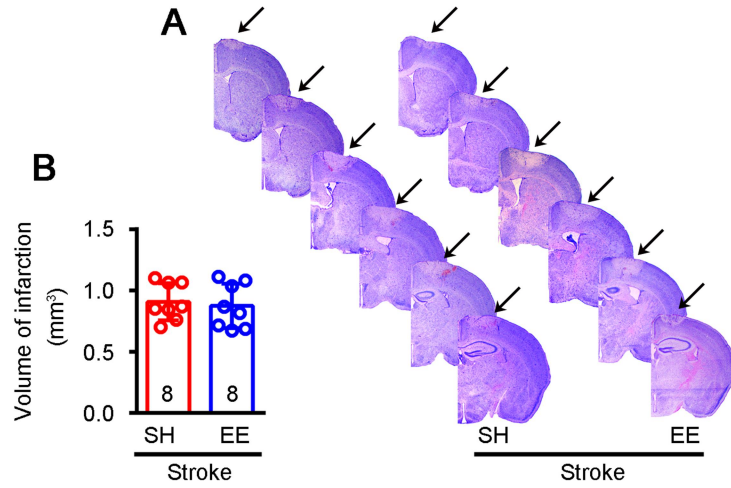


1 **Supplementary Figures**

2



3

4

5 **Figure S1. EE exposure 5–11 days after stroke has no effect on infarct size.**

6 **(A)** Representative Nissl-stained sections 12 days after stroke from Stroke + SH and

7 Stroke + EE mice. **(B)** Bar graph showing stroke volume in Stroke + SH and Stroke +

8 EE mice. Two tailed *t*-test, $F_{(1,14)} = 0.16$. EE, environmental enrichment; SH, standard

9 housing.

10

11

12

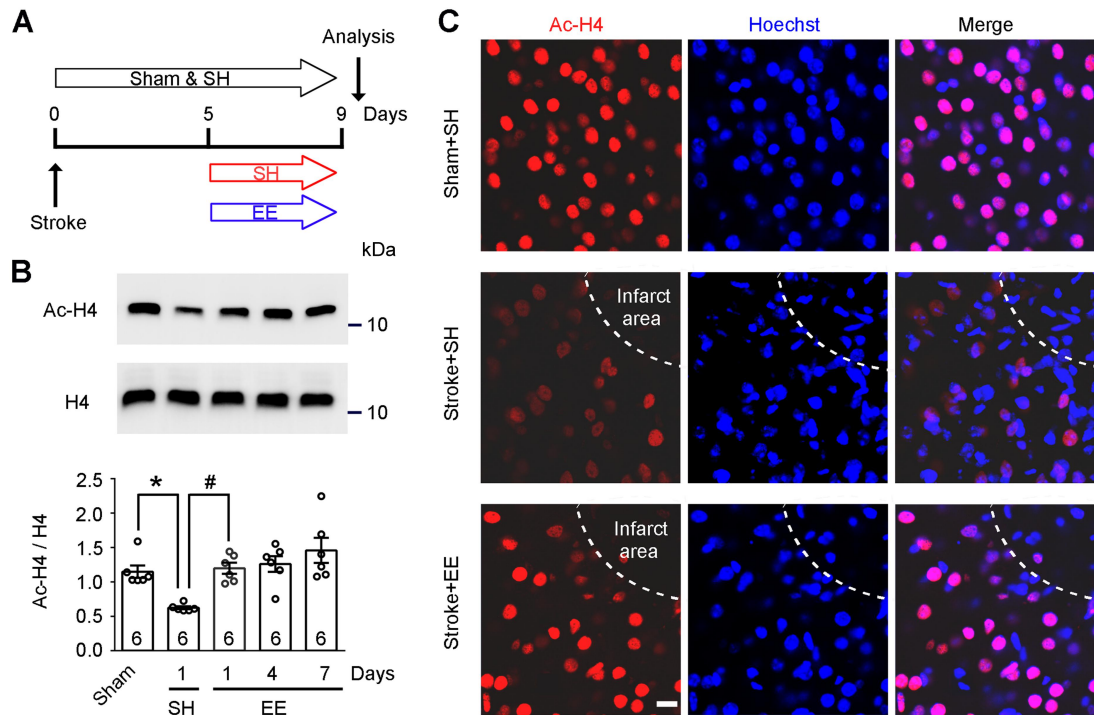
13

14

15

16

17



18

19

20 **Figure S2. EE exposure induces chromatin modifications in the peri-infarct area.**

21 **(A)** Experimental design for **(C)**. **(B)** Representative immunoblots and bar graph

22 showing the time course of acetyl-H4 levels in the peri-infarct cortex. Mice were

23 exposed to SH or EE 5 days after stroke. One-way ANOVA followed by post hoc

24 Scheffe test, $F_{(4,25)} = 7.81$, $*p = 0.048$, $\#p = 0.025$. **(C)** Representative

25 immunofluorescence images showing acetyl-H4 in the peri-infarct cortex. Scale bar,

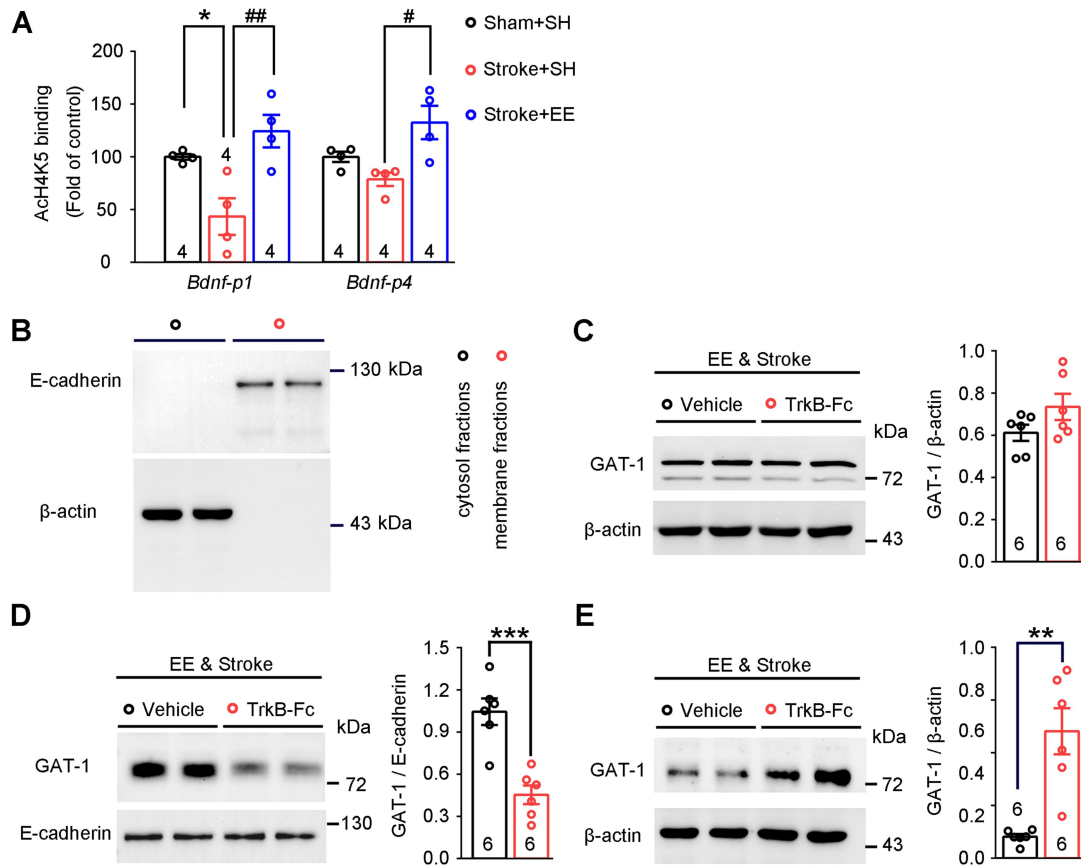
26 20 μm . EE, environmental enrichment; SH, standard housing.

27

28

29

30



31
32
33 **Figure S3. EE exposure primes a transcriptional program for the expression of**
34 **BDNF, which regulates trafficking of GAT-1.**

35 (A) Bar graph showing changes in histone acetylation in the promoter regions of
36 BDNF genes in peri-infarct tissue. Fragmented chromatin was immunoprecipitated
37 with antibody recognizing acetyl-H4 and quantified with real-time polymerase chain
38 reaction. One-way ANOVA followed by post hoc Scheffe test. For *Bdnf-p1*, $F_{(2,9)} =$
39 9.44, $*p = 0.047$, $##p = 0.007$; for *Bdnf-p4*, $F_{(2,9)} = 7.01$, $#p = 0.015$. (B) Confirmation
40 of the membrane protein fractions extraction method. Representative immunoblots
41 showing that β -actin was exclusively detected in cytosol fractions, while E-cadherin
42 was exclusively detected in membrane fractions. (C) Representative immunoblots and

43 bar graph showing GAT-1 content in peri-infarct cortex. Two-tailed *t*-test, $F_{(1,10)} =$
44 2.82. **(D)** Representative immunoblots and bar graph showing GAT-1 content in
45 membrane fraction. Two-tailed *t*-test, $F_{(1,10)} = 25.96$, $***p < 0.001$. **(E)** Representative
46 immunoblots and bar graph showing GAT-1 content in cytosol fractions. Two-tailed
47 *t*-test, $F_{(1,10)} = 20.58$, $**p = 0.001$. BDNF, brain-derived neurotrophicfactor.

48

49

50

51

52

53

54

55

56

57

58

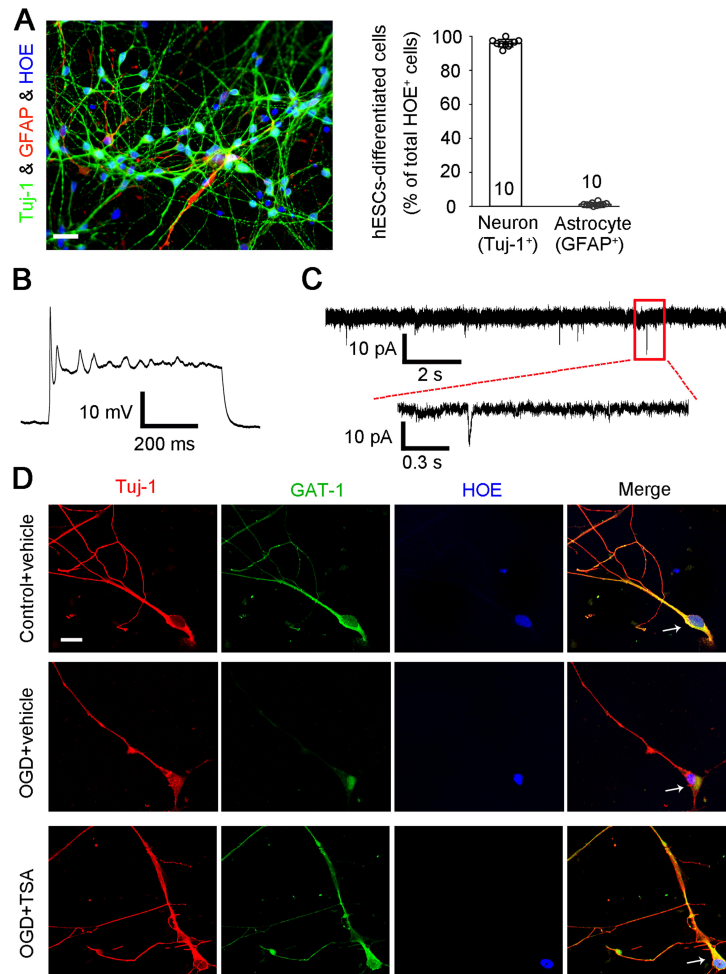
59

60

61

62

63



64

65

66 **Figure S4. TSA reverses OGD-induced internalization of GAT-1 in**
 67 **hESCs-derived neurons.**

68 (A) Representative fluorescence image and bar graph showing the percentage of
 69 neurons and astrocytes in hESCs-derived cells. Scale bar, 40 μ m. (B) Representative
 70 whole-cell patch clamp trace illustrating the number of APs in hESCs-derived neurons
 71 evoked by current injection. (C) Representative voltage clamp (-70 mV) traces
 72 showing hESCs-derived neurons displaying spontaneous postsynaptic currents. (D)
 73 hESCs-derived neurons were exposed to 3 h of OGD. TSA (0.5 μ M) was applied for
 74 24 h, starting 24 h after OGD. Representative fluorescence images showing Tuj-1 and

75 GAT-1 in hESCs-derived neurons at 48 h after OGD. Scale bar, 20 μ m. AP, action
76 potential; hESC, human embryonic stem cell; OGD, oxygen glucose deprivation; TSA,
77 trichostatin A.

78

79

80

81

82

83

84

85

86

87

88

89

90

91

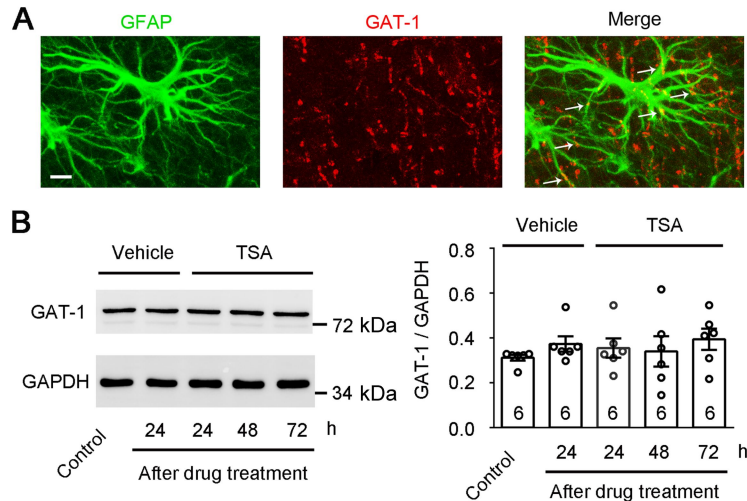
92

93

94

95

96



97

98

99 **Figure S5. OGD and TSA treatment have no effect on the expression of GAT-1 in**
 100 **astrocytes.**

101 **(A)** Representative fluorescence image showing GFAP (an astrocyte marker) and
 102 GAT-1 in the peri-infarct area. Arrows indicate GAT-1 co-localized with astrocytes.
 103 Scale bar, 20 μ m. **(B)** Cultured astrocytes were exposed to 3 h of OGD. TSA (0.5 μ M)
 104 was applied for 24, 48, and 72 h, starting 24 h after OGD. Immunoblots showing the
 105 time course of GAT-1 levels in cultured astrocytes after OGD exposure and TSA
 106 treatment. Bar graph showing the time course of GAT-1 levels in astrocytes after
 107 OGD exposure and TSA treatment. One-way ANOVA followed by post hoc Scheffe
 108 test, $F_{(4,25)} = 0.49$. OGD, oxygen glucose deprivation; TSA, trichostatin A.

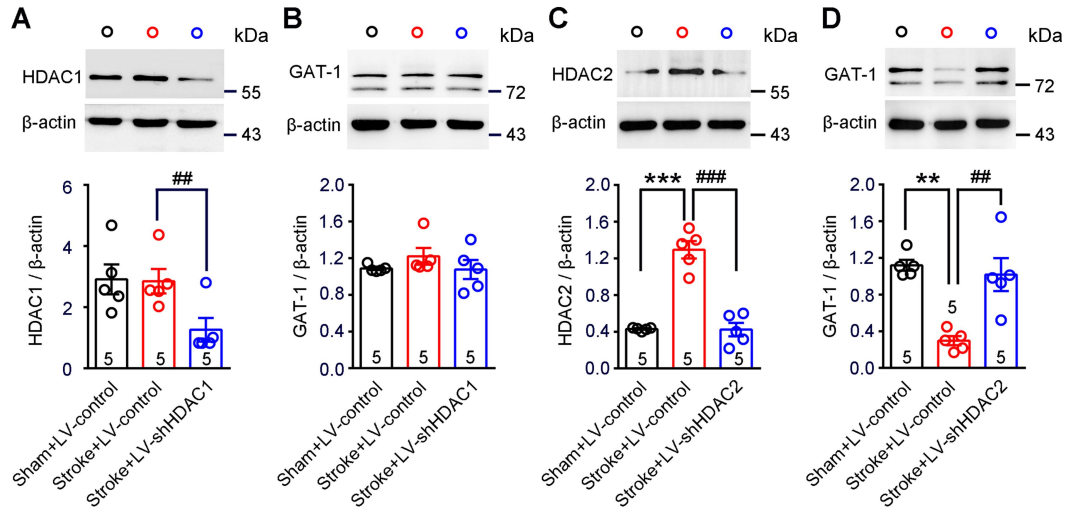
109

110

111

112

113



114

115

116 **Figure S6. HDAC2 but not HDAC1 negatively regulates GAT-1 expression.**

117 **(A)** Representative immunoblots and bar graph showing HDAC1 content in the

118 peri-infarct cortex 5 days after stroke. One-way ANOVA followed by post hoc Scheffe

119 test, $F_{(2,12)} = 10.18$, $^{##}p = 0.008$. **(B)** Representative immunoblots and bar graph

120 showing GAT-1 content in the peri-infarct cortex 5 days after stroke. One-way

121 ANOVA followed by post hoc Scheffe test, $F_{(2,12)} = 1$. **(C)** Representative

122 immunoblots and bar graph showing HDAC2 content in the peri-infarct cortex 5 days

123 after stroke. One-way ANOVA followed by post hoc Scheffe test, $F_{(2,12)} = 52.41$, $^{***}p$

124 < 0.001 , $^{###}p < 0.001$. **(D)** Representative immunoblots and bar graph showing GAT-1

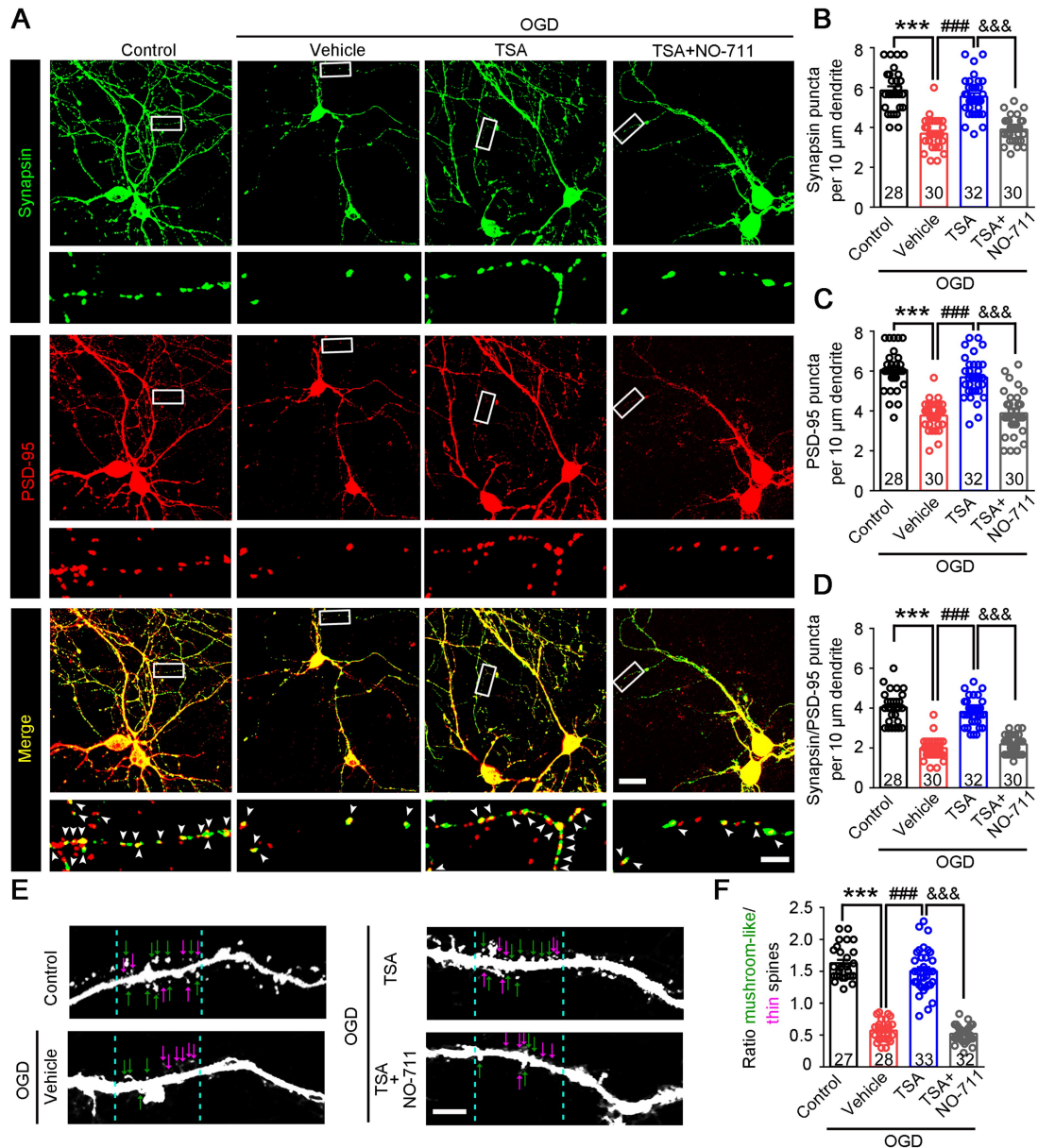
125 content in the peri-infarct cortex 5 days after stroke. One-way ANOVA followed by

126 post hoc Scheffe test, $F_{(2,12)} = 15.75$, $^{**}p = 0.001$, $^{##}p = 0.003$. HDAC, histone

127 deacetylase.

128

129



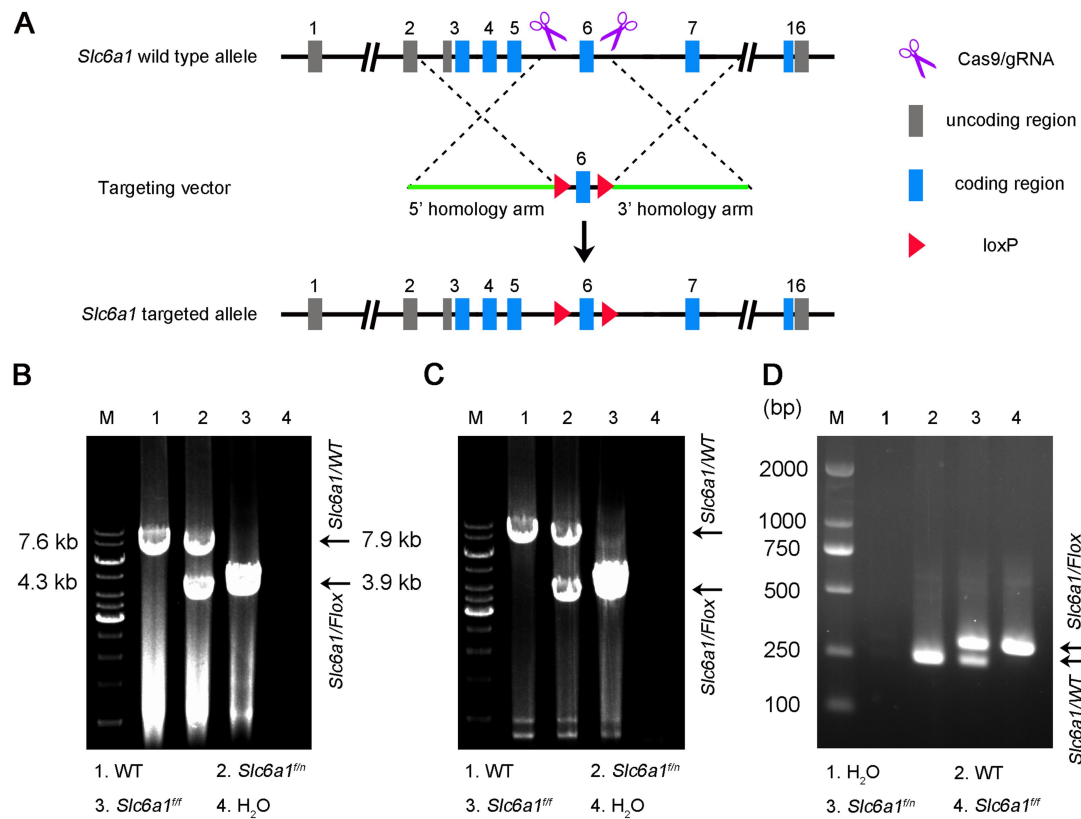
130

131

132 **Figure S7. GAT-1 is critical for the TSA-mediated increase in dendritic spine**
 133 **density and synaptogenesis after hypoxia.**

134 **(A)** Primary cultured mouse cortical neurons were exposed to 3 h of OGD. TSA (0.5
 135 μ M) or a mixture of TSA (0.5 μ M) and NO-711 (10 μ M) was applied for 24 h, starting
 136 24 h after OGD. Representative fluorescence image showing synapsin and PSD-95 in
 137 primary cultured mouse cortical neurons after OGD. Each lower panel is a magnified

138 selected area from the upper image showing dendritic spines. Arrows indicate
139 synapsin / PSD-95 double-positive puncta. Upper scale bars, 20 μm . Lower scale bars,
140 5 μm . **(B)** Bar graph showing the average density of synapsin puncta in dendritic
141 segments of primary cortical neurons of the indicated groups. One-way ANOVA
142 followed by post hoc Scheffe test, $F_{(3,116)} = 46.37$, $***p < 0.001$, $###p < 0.001$, $***p < 0.001$, $***p < 0.001$. n indicates the number of dendrites from 3 independent experiments. **(C)** Bar
143 graph showing the average density of synapsin puncta in dendritic segments of
144 primary cortical neurons with the indicated treatments. One-way ANOVA followed by
145 post hoc Scheffe test, $F_{(3,116)} = 40.74$, $***p < 0.001$, $###p < 0.001$, $***p < 0.001$. **(D)** Bar
146 graph showing the average density of synapsin / PSD-95 colocalized puncta in
147 dendritic segments of primary cortical neurons with the indicated treatments.
148 One-way ANOVA followed by post hoc Scheffe test, $F_{(3,116)} = 82.06$, $***p < 0.001$, $###p$
149 < 0.001 , $***p < 0.001$. **(E)** Representative images of primary cultured cortical
150 neurons infected with LV-GFP showing the morphology at 48 h after OGD. Scale bar,
151 5 μm . **(F)** Bar graph showing the ratio of mushroom-like spines versus thin spines in
152 the indicated groups. One-way ANOVA followed by post hoc Scheffe test, $F_{(3,116)} =$
153 170.22 , $***p < 0.001$, $###p < 0.001$, $***p < 0.001$. n indicates the number of dendrites
154 from 3 independent experiments. OGD, oxygen glucose deprivation; TSA, trichostatin
155 A.
156
157
158



159

160

161 **Figure S8. Generation of GAT-1^{flox/flox} mice.**

162 **(A)** Schematic illustration of the *Slc6a1* gene, targeting vector and the *Slc6a1* floxed

163 locus. The *Slc6a1* gene has 16 exons, and exon 6 was floxed to generate GAT-1^{flox/flox}

164 mice. **(B)** ES clones with 5' arm homologous recombination were confirmed by PCR

165 verification with a 4.3 kb band, while wild type generated a 7.6 kb band. **(C)** ES

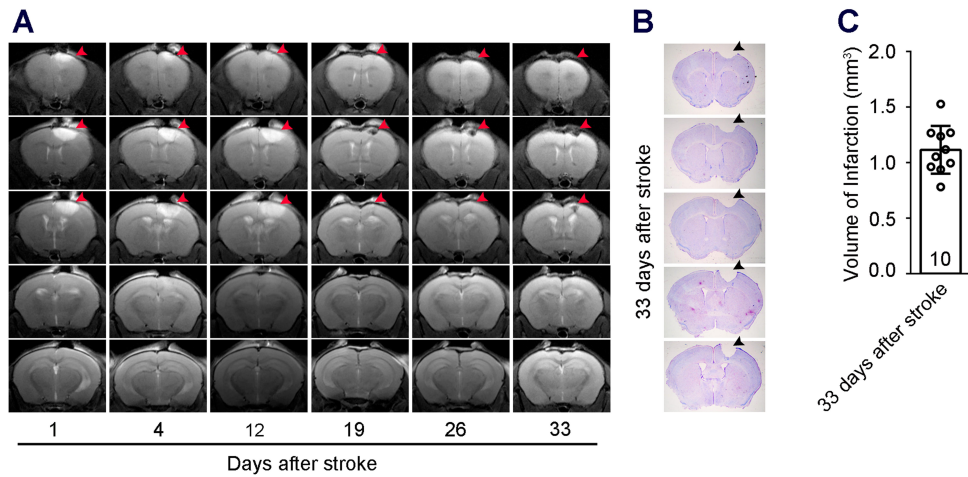
166 clones with 3' arm homologous recombination were confirmed by PCR verification

167 with a 3.9 kb band, while wild type generated a 7.9 kb band. **(D)** Genotyping of

168 GAT-1^{flox/flox} mice. DNA was isolated for PCR with two primer pairs. The GAT-1

169 primers generated a 304 bp product in the loxP-flanked allele or a 246 bp product in

170 the wild-type allele. M, marker; PCR, polymerase chain reaction.



171

172

173 **Figure S9. Phot thrombotic stroke model induces long-lasting motor cortex**
 174 **injury in adult mice.**

175 (A) Time course of representative T2-TurboRARE MRI of phot thrombotic stroke
 176 mice. Arrows indicate the injured areas. (B) Representative Nissl-stained sections on
 177 day 33 after stroke. Arrows indicate the injured areas. (C) Bar graph showing stroke
 178 volume.

179

180

181

182

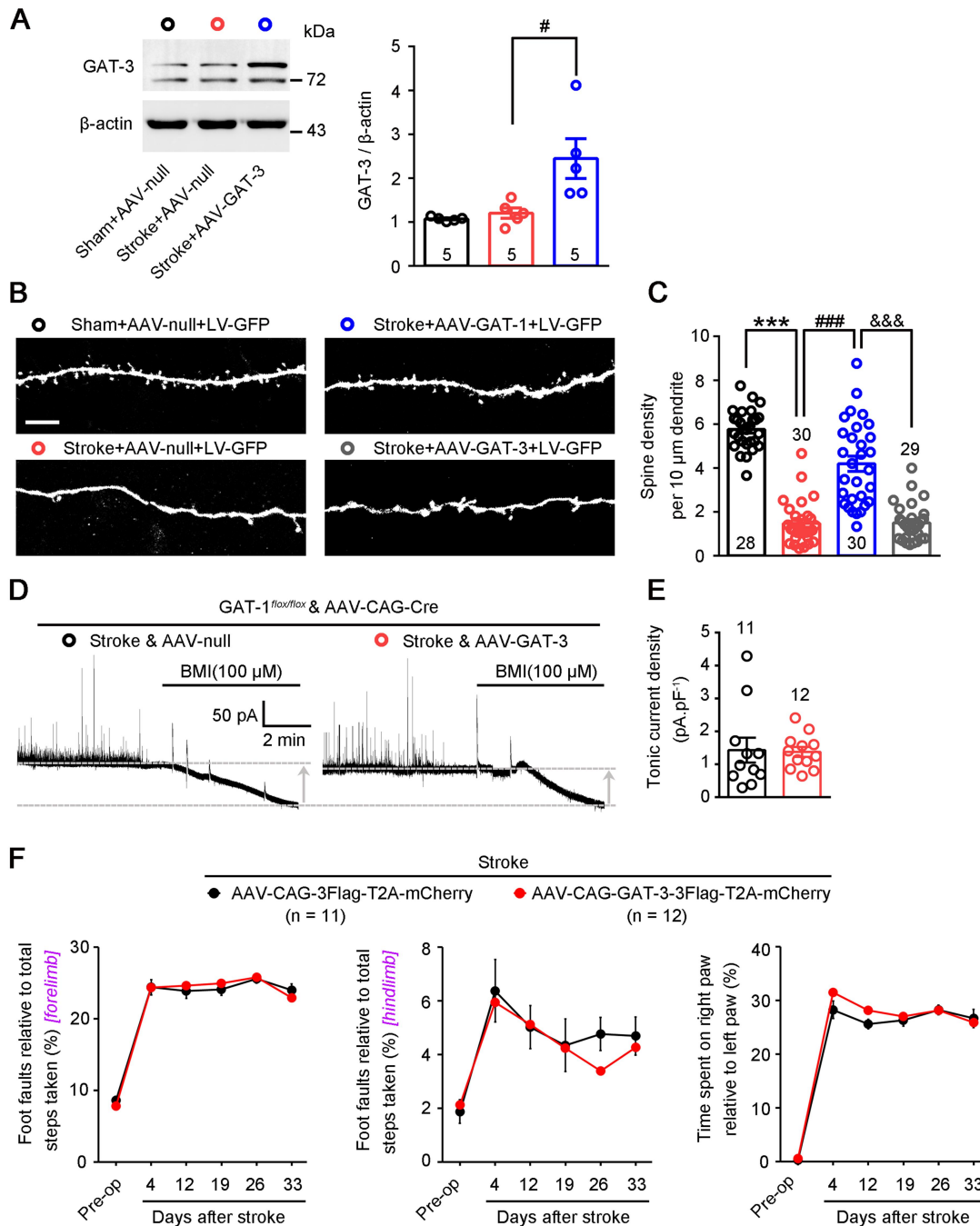
183

184

185

186

187



188

189

190 **Figure S10. GAT-1 but not GAT-3 overexpression promotes stroke recovery.**

191 (A) GAT-3 level in the peri-infarct cortex 8 days after AAV-CAG-3Flag-T2A-mcherry

192 (AAV-null) or AAV-CAG-GAT-3-3Flag-T2A-mcherry (AAV-GAT-3) infection.

193 One-way ANOVA followed by post hoc Scheffe test, $F_{(2,12)} = 7.87$, # $p = 0.023$. (B)

194 Representative images showing the dendritic spines of peri-infarct neurons infected

195 with AAV-null, AAV-GAT-1 or AAV-GAT-3. For spine density analysis, only apical
196 dendrites of layer 5 pyramidal neurons in the peri-infarct cortex (within 400 μm from
197 the infarct) were included. Scale bar, 5 μm . **(C)** Bar graph showing spine densities of
198 the indicated group. One-way ANOVA followed by post hoc Scheffe test, $F_{(3,113)} =$
199 83.71, $***p < 0.001$, $###p < 0.001$, $\&\&\&p < 0.001$. n indicates the number of dendrites
200 from 3 independent experiments. **(D)** Representative traces showing tonic inhibitory
201 currents recorded from layer 5 pyramidal neurons in AAV-null- or
202 AAV-GAT-3-infected GAT-1 knockdown mice. **(E)** Bar graph showing tonic current
203 density from layer 5 pyramidal neurons in AAV-null- or AAV-GAT-3-infected GAT-1
204 knockdown mice. Two-tailed t -test, $F_{(1,21)} = 0.02$. **(F)** Left, foot faults of the left
205 forelimb in the grid-walking task. Middle, foot faults of the left hindlimb in the
206 grid-walking task. Right, forelimb symmetry in the cylinder task. Two-way
207 repeated-measures ANOVA followed by post hoc Bonferroni test. Left, $F_{(1,22)} = 0.001$.
208 Middle, $F_{(1,22)} = 0.353$. Right, $F_{(1,22)} = 1.537$. AAV, adeno-associated virus; BMI,
209 bicuculline methiodide.
210